Marine Energy Research

SCIEPublish

Article

# Multi-Objective Optimization of Inverter Siting and Collector-Cable Routing for Fixed-Topology Offshore Floating Photovoltaic Plants with Inter-Block Gap Allowance

**Yan Zhang [1,2], Xiangyu Kong [1,3], Pengfei Li [1,*], Zilong Yu [1] and Zhenglong Yang [4]**

[1] Tianjin Key Laboratory of New Energy Power Conversion, Transmission and Intelligent Control, Tianjin University of Technology, Tianjin 300384, China; zhangyan1856@stud.tjut.edu.cn (Y.Z.); eekongxy@tju.edu.cn (X.K.); yuzilong0607@163.com (Z.Y.)

[2] School of Ocean Energy, Tianjin University of Technology, Tianjin 300384, China

[3] National Industry-Education Platform of Energy Storage, Tianjin University, Tianjin 300072, China

[4] National Science Center for Earthquake Engineering, Tianjin University, Tianjin 300350, China; nfees@tju.edu.cn (Z.Y.)

* Corresponding author. E-mail: pengfeili_ee@email.tjut.edu.cn (P.L.)

Received: 28 August 2026; Revised: 7 September 2026; Accepted: 8 October 2026; Available online: 15 October 2026

**ABSTRACT:** Offshore floating photovoltaic (OFPV) plants require cable allowance at interfaces between floating blocks to support maintenance access and accommodate relative motion. Because synchronized relative-motion records are often unavailable during early design, this allowance cannot be calibrated directly. This study proposes a fixed-topology multi-objective method for joint inverter siting and low-voltage collector-cable routing. CAD polylines are decomposed into fixed segments, and route-specific inter-block crossings, and a bounded gap-allowance factor is applied only at the crossings. NSGA-II generates nondominated layouts that minimize cable investment and the present value of resistive-loss cost while satisfying equipment-capacity, string-count, current, and voltage-drop constraints. The method is applied to a 5.1212 MWp grid-connected OFPV plant under the nominal routing case ($\gamma_s = 1$). Compared with the manual design, the selected compromise layout reduces collector-cable investment by 7.0% and the present value of power-loss cost by 14.9%, producing a 9.76% reduction in the modeled total collection-system cost. The results demonstrate the economic value of coordinated inverter siting and cable routing while identifying the data required for future dynamic-allowance calibration.

**Keywords:** Offshore floating photovoltaic; Inverter placement; Collector-cable routing; Inter-block gap allowance; Multi-objective optimization

## 1. Introduction

### *1.1. Background and Motivation*

Offshore floating photovoltaic (OFPV) technology can expand renewable-energy capacity without occupying land [1,2]. Unlike protected inland waters, offshore sites expose floating arrays to waves, tides,

© 2026 The authors. This is an open access article under the Creative Commons Attribution 4.0 International License (https://creativecommons.org/licenses/by/4.0/).

salt spray, wind-wave interaction, and restricted maintenance access. These conditions impose stricter requirements on structural integrity and electrical reliability [3]. Platform configuration and tidal variation affect the motion of multi-module systems [4], hydroelastic response can amplify local loads and failure modes [5], and mooring design governs station keeping under offshore environmental loads [6]. Collector-cable layout is therefore part of the integrated OFPV design problem rather than a purely static geometric exercise. In the fixed-topology problem considered here, the generating-array partition, transformer locations, feeder topology, and equipment specifications are prescribed. The remaining decisions are the inverter location in each array and the associated low-voltage Direct Current (DC) and Alternating Current (AC) routes. These decisions determine installed cable length, investment, resistive losses, and voltage drop. A route that crosses several floating-block interfaces also requires service allowance at those interfaces, whereas a route confined to one block does not.

### *1.2. Related Work and Research Gap*

Relevant studies first arise from structural and cable engineering. A pontoon–truss OFPV concept with soft connections has been developed and tested experimentally [7], demonstrating the importance of modular interfaces in offshore layouts. For floating offshore wind systems, suspended inter-array cable configurations have been optimized with explicit platform-motion constraints [8], providing a useful mechanical analogue for OFPV connections. Other studies have examined submarine-cable ampacity in marine environments [9], the performance and design of floating photovoltaic (PV) systems [10], and the influence of floating support structures on equipment layout and cable routes [11]. These studies clarify environmental, structural, and electrical requirements, but they do not translate the number of floating-block interfaces crossed by each candidate route into a plant-level collector-system optimization variable.

A second research direction concerns electrical-network planning and multi-objective optimization. Integrated models have coordinated cable-network layout, conductor cross-sections, and substation locations for offshore wind farms [12]. For OFPV systems, plant capacity and configuration have been formulated as an NSGA-II problem [13], while offshore-wind cable studies provide established methods for route decisions and network-cost evaluation [14]. Reviews of multi-objective optimization [15] and NSGA-II for combinatorial problems [16], together with the original NSGA-II formulation and subsequent variants [17–19], provide the methodological basis for balancing investment and performance. Related multi-objective and techno-economic applications appear in energy forecasting and floating PV studies [20–22]. However, existing electrical-layout models typically use static routing distances, whereas dynamic-cable studies emphasize mechanical configuration. Few studies jointly consider inverter placement, route-specific floating-block crossings, and the combined economics of the DC and low-voltage AC collection system.

### *1.3. Scope and Main Contributions*

This paper addresses the following scoped design problem: for prescribed generating-array boundaries, transformer locations, feeder topology, inverter type, and cable specifications, select one feasible inverter location in each array and evaluate its associated DC and AC collector routes. The main contributions are as follows. (1) A CAD-informed, route-specific inter-block gap-allowance model is developed by separating each nominal route into fixed segments and floating-block boundary crossings. The allowance factor is applied only to the latter and is treated as a bounded design parameter rather than an experimentally calibrated wave-response coefficient. (2) Cable investment and present-value life-cycle loss cost are formulated as separate objectives subject to equipment, string-count, current, and voltage-drop constraints. NSGA-II is used as a mature solver to generate nondominated inverter-location layouts rather than being claimed as a new algorithmic contribution. (3) The validation scope is made explicit through CAD-

geometry, dimensional consistency, limiting-case, and monotonicity checks. The quantitative results correspond only to $\gamma_s = 1$; $\gamma_s > 1$ values are defined as a prospective sensitivity protocol because synchronized adjacent-block relative-motion data are unavailable. (4) The method is demonstrated using a 5.12 MWp OFPV plant with 14 generating arrays and two fixed box-type transformers. Under the nominal routing scenario, the selected scheme reduces the modeled collector-cable cost components by 9.76% relative to the manual design.

### *1.4. Paper Organization*

The remainder of this article is organized as follows. Section 2 defines the OFPV collection system and optimization framework. Section 3 presents the inter-block gap-allowance model, objective functions, constraints, and NSGA-II procedure. Section 4 describes the 5.1212 MWp case study and discusses the results and limitations. Section 5 summarizes the conclusions and future work.

## 2. Offshore Floating PV Electrical Collection System and Optimization Framework

This section establishes the electrical architecture, spatial abstraction, and optimization workflow used in the remainder of the paper. The description proceeds from the plant-level energy path to the generating-array interfaces and then to the route variables and objective functions. The system boundary follows the offshore FPV equipment interfaces identified in recent comparative floating-PV studies [22]. The same coordinate definitions are used for the nominal CAD routes and the route-specific inter-block allowance. The present optimization focuses on the DC cables from PV strings to string inverters and the low-voltage AC cables from string inverters to the box-type transformers. The downstream 35-kV collector feeders are treated as fixed-topology components and are not included as decision variables.

### *2.1. OFPV Electrical Collection-System Architecture*

An OFPV plant integrates the PV generating system, floating-platform structure, mooring system, string inverters, box-type transformers, dynamic submarine cables, the onshore substation, and the grid connection. The floating platforms are grouped into modular generating arrays. As shown in Figure 1, PV power is converted and stepped up on the floating side, transmitted via the dynamic cable, and delivered to the substation prior to grid connection. This plant-level architecture defines the equipment interfaces considered in the optimization.

The design variables are the inverter locations and the associated DC and AC cable routes within the generating arrays. The electrical model must simultaneously account for the nominal geometry, the available routing corridors, and the additional service allowance required at interfaces between moving floating blocks, consistent with the cable-configuration problem reported for floating offshore networks [23,24]. The nonlinear bending behavior of dynamic submarine power cables also needs to be considered when a detailed mechanical design is performed [25]. Because such a mechanical calibration is outside the available data set, the present study introduces a bounded, route-specific gap allowance and explicitly states its validation scope below.

The simplified electrical path in Figure 2 is consistent with the plant-level architecture. PV strings deliver low-voltage DC power to the inverter. After conversion and voltage step-up through the subsequent AC interface, medium-voltage AC power is transmitted toward the substation. The figure is used only to identify the energy-flow direction and voltage-level transition; the detailed cable-length calculation is performed using the array-level route model below.

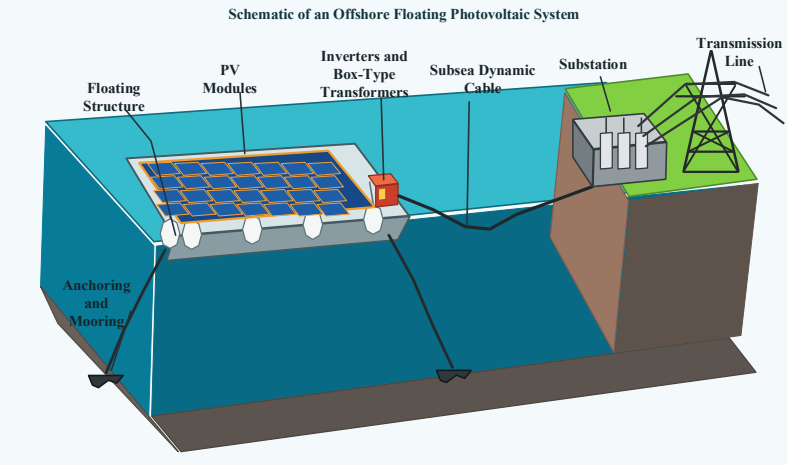


**Figure 1.** OFPV system composition and plant-level energy-transfer path.

Figure 1 gives the system boundary, whereas Figure 2 gives the simplified electrical connection used to explain the route classes. In an engineering layout, flexible connectors, cable carriers, maintenance corridors, minimum bending radii, separation distances, corrosion protection, and access requirements must also be satisfied. These conditions are retained as feasibility requirements rather than being treated as decorative elements of the schematic.

At the generating-array level, the local interfaces among PV strings, the string inverter, the box-type transformer, and the collector feeder are represented separately. This separation distinguishes the string-to-inverter DC routes from the inverter-to-transformer AC routes and provides the coordinate basis for calculating their lengths and losses.

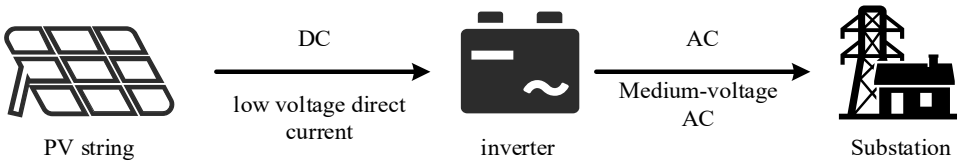


**Figure 2.** Simplified electrical connection and voltage-level transition.

## *2.2. Proposed Optimization Framework*

As summarized in Figure 3, the method has four stages. (1) The plant architecture, array partition, equipment data, and candidate inverter positions are defined. (2) The CAD-informed gap-aware Manhattan model converts each candidate route into a serviceable cable length by separating fixed segments from inter-block crossings. (3) DC/AC investment costs, resistive losses, and electrical constraints are evaluated for the resulting layout. (4) NSGA-II generates and ranks nondominated layouts, after which a representative solution is selected using engineering feasibility and life-cycle economy. The integrated separation of network layout, cable selection, and substation-related decisions is consistent with recent integrated electrical-collection optimization practice [12].

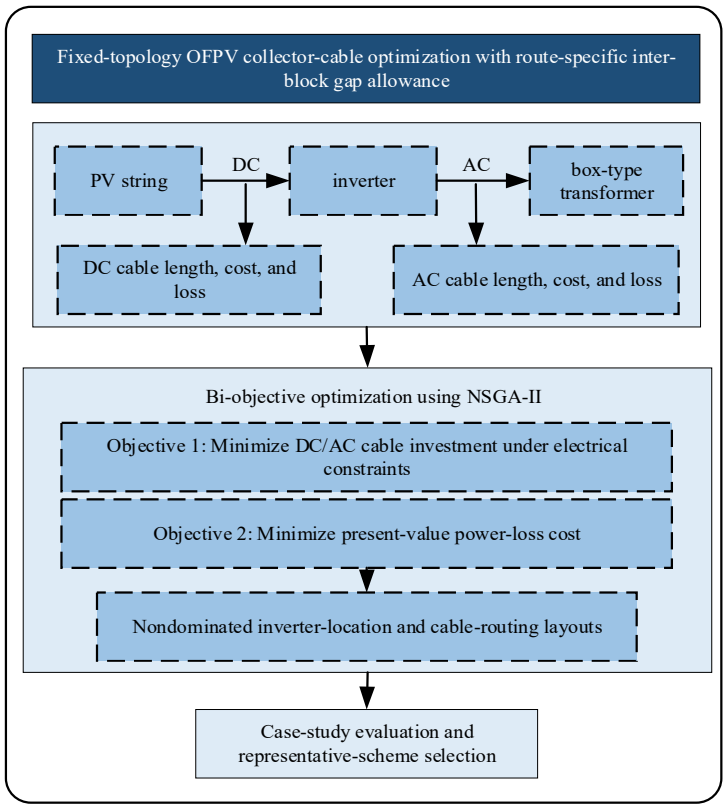


**Figure 3.** Research framework for fixed-topology OFPV collector-cable optimization. Route geometry and inter-block crossings are evaluated before the electrical-economic objectives are passed to NSGA-II.

## 3. Hierarchical Multi-Objective Optimization Strategy for the OFPV Collection System

The collection-system design is formulated around coupled discrete decisions. In the present case study, the array division, transformer locations, inverter type, and cable specifications are fixed, while one feasible inverter position is selected in each generating array. For each chromosome, the corresponding DC and AC route lengths are calculated using the route-specific inter-block gap-allowance model, and the resulting electrical and economic quantities are passed to the system-level multi-objective search. The use of a Pareto search for floating offshore PV sizing and configuration is also consistent with recent reliability-oriented offshore design studies [26].

### *3.1. Route-Specific Inter-Block Gap-Allowance Model*

Standardizing the generating arrays of an OFPV plant enables regular cable corridors and can simplify design, installation, operation, and maintenance. Cables from PV strings can be routed along support beams within each row and secured using nylon straps or equivalent fasteners. The case-study electrical drawing represents the collection routes as measurable orthogonal polylines and separately identifies the string-to-inverter and inverter-to-transformer interfaces. Manhattan distance is therefore retained as an engineering abstraction for the nominal grid route, while additional cable allowance is assigned only to route segments that cross floating-block interfaces. Reference [27] is used only to support the need for dynamic inter-array cable design considerations, not the Manhattan-grid assumption.

Let $P_1 = (x_1, y_1)$ and $P_2 = (x_2, y_2)$ denote two points on an orthogonal grid. Their Manhattan distance is the sum of the absolute horizontal and vertical coordinate differences, as expressed in Equation (1):

$$D = |x_1 - x_2| + |y_1 - y_2| \quad (1)$$

In the conventional model, any monotonic orthogonal path between two points has a length equal to the sum of the absolute horizontal and vertical displacements. In Figure 4, paths A and C follow different orthogonal routes but have identical Manhattan distances, whereas path B represents the Euclidean distance. A single global multiplier applied to every route would preserve the route ranking and would not distinguish a route that remains on one floating block from a route that crosses many block interfaces. The nominal route is therefore decomposed into fixed segments and route-specific inter-block gap crossings.

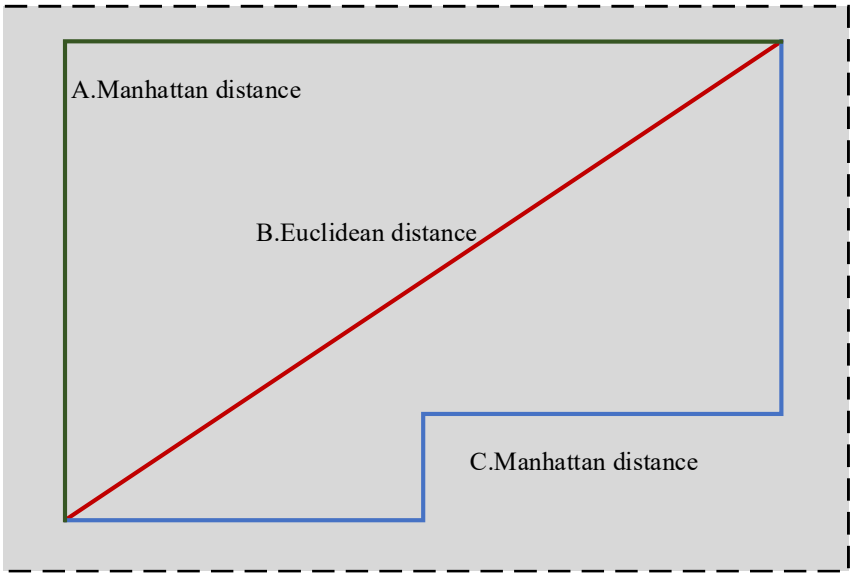


**Figure 4.** Comparison of Manhattan and Euclidean routes.

For route $r$, the CAD polyline length is denoted by $L_r^{CAD}$, and $N_r$ is the number of times that the route intersects a floating-block boundary. The nominal prototype gap is $d_0$. Only the $N_r$ crossing segments require an additional flexibility allowance; the remaining route length is treated as fixed to the support structure.

The fixed portion of route $r$ is defined by Equation (2):

$$L_r^{fix} = L_r^{CAD} - N_r d_0 \tag{2}$$

where $L_r^{fix}$ is the cable length fixed to modules, beams, trays, or other supports; $L_r^{CAD}$ is the nominal route length extracted from the electrical drawing; $N_r$ is the route-specific number of inter-block crossings; and $d_0$ is the nominal gap. For allowance scenario $s$, the total length assigned to the crossing segments is defined by Equation (3):

$$L_{r,s}^{gap} = \gamma_s \, N_r \, d_0, \quad \gamma_s \geq 1 \tag{3}$$

where $L_{r,s}^{gap}$ is the scenario-dependent length assigned to all gap crossings, and $\gamma_s \geq 1$ is a dimensionless flexibility-allowance factor. The factor is not calculated from significant wave height alone and is not interpreted as a hydrodynamic response coefficient.

The resulting serviceable route length is given by Equation (4), and the associated fixed-segment/inter-block-crossing decomposition is illustrated in Figure 5:

$$L_{r,s}^{design} = L_r^{fix} + L_{r,s}^{gap} = L_r^{CAD} + (\gamma_s - 1) N_r \, d_0 \tag{4}$$

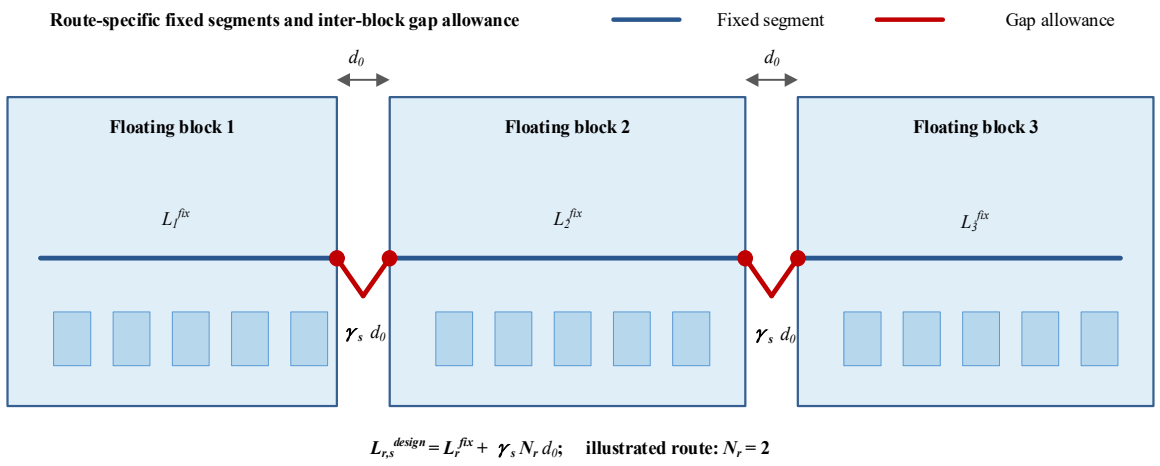


**Figure 5.** Route-specific decomposition of a collector-cable route. Fixed segments remain on the floating blocks, while allowance $\gamma_s d_0$ is assigned at each of $N_r$ inter-block crossings.

### 3.1.1. Engineering Verification and Validation Scope

The case-study electrical drawing contains measurable orthogonal route polylines, numbered inverter interfaces for the 14 generating arrays, and two 2500 kVA box-type transformers. For a finalized routing dataset, $L_r^{CAD}$ is obtained from each CAD polyline, and $N_r$ is obtained by intersecting that route with the floating-block boundaries. The geometric input must satisfy $L_r^{CAD} \geq N_r d_0$, and the polyline length must equal the sum of its orthogonal segments within the drawing tolerance. The Pareto and cost results use $\gamma_s = 1$, for which Equation (4) reduces to the nominal CAD route and no unmeasured dynamic displacement is introduced.

The case-study environmental design basis includes a significant wave height of 2.10 m, a peak period of 10.19 s, a maximum wave height of 3.50 m, a 50-year daily maximum wind speed of 32.63 m/s, and a maximum current speed of 1.378 m/s. The corresponding 1:25 physical-model configuration used a 2 mm inter-block gap, equivalent to a prototype nominal gap of 0.05 m. Wind and current loads may cause platform offset, rotation, and relative motion between adjacent floating blocks, thereby affecting the free cable length, tension, bending, and fatigue at inter-block crossings. In the present study, however, the wind and current values define the mechanical design environment and are not used as direct numerical inputs to the electrical-economic optimization. Quantifying these mechanical effects would require a coupled floating-structure, mooring, and cable analysis. Because synchronized relative-displacement histories are unavailable, $\gamma_s$ is treated as a prescribed design-allowance factor rather than a hydrodynamically calibrated coefficient.

Three limiting checks establish the internal behavior of the formulation. When $\gamma_s = 1$, Equation (4) reduces exactly to the nominal CAD route; when $N_r = 0$, a route located entirely on one floating block is unchanged; and for $N_r > 0$, the serviceable length increases monotonically with $\gamma_s$. The bounded set $\gamma_s = \{1.00, 1.25, 1.50, 2.00\}$ defines a prospective sensitivity protocol for additional allowances of 25%, 50%, and 100% over the nominal crossing length. Because all numerical results use the nominal case $\gamma_s = 1$, route-specific crossing counts do not introduce any additional gap allowance into the calculated cable lengths. Evaluating $\gamma_s > 1$ would require finalized crossing counts for each candidate route and synchronized relative-motion data for adjacent blocks; therefore, the present study does not report a completed dynamic-allowance sensitivity analysis.

These checks establish route-model consistency and delimit the available engineering evidence; they do not constitute direct physical validation of dynamic cable tension, curvature, minimum bending radius, or fatigue. Such validation requires synchronized adjacent-block motion histories and a coupled hydrodynamic–dynamic-cable model or dedicated cable tests.

### 3.1.2. DC Cable Costs and Losses

Within a generating array, $n$ PV strings are connected to one inverter. A common coordinate system is established for the string terminals, candidate inverter positions, route polylines, and floating-block boundaries. Using Equation (4) for each string route, the total DC cable length under allowance scenario $s$ is calculated using Equation (5):

$$L_{DC,s} = \sum_{i=1}^{n} (L_i^{fix} + \gamma_s \, N_i \, d_0) \tag{5}$$

where $L_{DC,s}$ denotes the total scenario-dependent DC cable length; $L_i^{fix}$ is the fixed portion of the route from PV string $i$ to its inverter; $N_i$ is the number of floating-block boundaries crossed by that route; $d_0$ is the nominal gap; and $n$ is the number of PV strings in the generating array.

DC cable investment is proportional to the installed scenario-dependent cable length, while the unit price depends on the conductor cross-sectional area. The total DC cable cost is calculated using Equation (6):

$$C_{DC,s} = P_{dc} L_{DC,s} \tag{6}$$

where $P_{dc}$ denotes the unit price of the DC cable and $L_{DC,s}$ is the serviceable DC cable length from Equation (5). No additional global cable-length multiplier is applied.

DC-side cable losses are dominated by conductor resistance and are calculated using Equation (7):

$$P_{loss,dc} = I_{dc}^2 \times R_{dc} \times L_{DC,s} \tag{7}$$

where $I_{dc}$ denotes the DC current; $R_{dc}$ denotes the cable resistance per unit length.

### 3.1.3. AC Cable Costs and Losses

The inverter location within each generating array affects the low-voltage AC cable length, cable investment, resistive losses, and system efficiency. Each array contains one string inverter that aggregates the outputs of its PV strings. The inverter-to-transformer route is decomposed using the same fixed-segment and inter-block-crossing definitions. The total low-voltage AC cable length and cost are calculated using Equations (8) and (9), respectively. The downstream 35-kV cables from the box-type transformers to the branch boxes and switch station remain fixed and are not included among the optimization variables:

$$L_{AC,s} = \sum_{j=1}^{m} (L_j^{fix} + \gamma_s \, N_j \, d_0) \tag{8}$$

$$C_{AC,s} = P_{ac} L_{AC,s} \tag{9}$$

where $L_{AC,s}$ denotes the total serviceable low-voltage AC cable length from the $m$ inverters to the two fixed box-type transformers; $L_j^{fix}$ and $N_j$ denote the fixed length and inter-block crossing count of inverter route $j$, respectively; and $P_{ac}$ denotes the unit price of the AC cable.

AC-side cable losses are dominated by conductor resistance and are calculated using Equation (10):

$$P_{loss,ac} = 3 \times I_{ac}^2 \times R_{ac} \times L_{AC,s} \tag{10}$$

where $I_{ac}$ denotes the rms phase current; $R_{ac}$ denotes the cable resistance per unit length; and $L_{AC,s}$ denotes the scenario-dependent low-voltage AC cable length from the inverter outputs to the low-voltage sides of the box-type transformers.

### *3.2. Constraint Conditions*

Electrical-collection-system design must satisfy line-loss, voltage-drop, equipment, safety, environmental, material, economic, and future-expansion requirements. The numerical comparison evaluates the nominal route lengths. If the prospective allowance cases are evaluated after route-specific crossing counts become available, the length-dependent loss and voltage-drop constraints must be recalculated using $L_{DC,s}$ and $L_{AC,s}$ for every case. The remaining constraints are summarized below.

(1) Major electrical equipment for an OFPV plant must be selected for reliable operation under offshore conditions, including elevated temperature, salt fog, and vibration. Equipment ratings are determined from the operating environment, short-circuit calculations, and expected operating modes.

(2) For a given installed capacity, the number of modules per PV string is maximized subject to the inverter input-voltage and MPPT-voltage limits. The admissible range is defined by Equations (11) and (12):

$$N \le \frac{V_{dc\max}}{V_{oc} \times [1 + (t - 25) \times K_v]} \tag{11}$$

$$\frac{V_{MPPT\min}}{V_{pm} \times [1 + (t' - 25) \times K'_v]} \le N \le \frac{V_{MPPT\max}}{V_{pm} \times [1 + (t - 25) \times K'_v]} \tag{12}$$

where $N$ denotes the number of PV modules connected in series; $K_v$ denotes the open-circuit-voltage temperature coefficient; $K'_v$ denotes the operating-voltage temperature coefficient; $t$ denotes the minimum module operating temperature; $t'$ denotes the maximum module operating temperature; $V_{dc\max}$ denotes the maximum permissible inverter DC input voltage; $V_{MPPT\max}$ denotes the upper limit of the inverter MPPT-voltage range; $V_{MPPT\min}$ denotes the lower limit of the inverter MPPT-voltage range; $V_{oc}$ denotes the module open-circuit voltage; and $V_{pm}$ denotes the module operating voltage.

(3) Under standard test conditions, the voltage drop from each PV string to the inverter DC input and from each inverter AC output to the transformer low-voltage side must not exceed 1.0%. The DC voltage-drop constraint is expressed by Equation (13):

$$\Delta V_{dc} = \frac{2 \cdot I_{mp} \cdot R_{dc} \cdot L_{dc}}{V_{dc,nom}} \times 100\% \le 1\% \tag{13}$$

where $I_{mp}$ denotes the PV-string current at the maximum power point under standard test conditions; $R_{dc}$ denotes the DC cable resistance per unit length; $L_{dc}$ denotes the one-way cable length and is set equal to the applicable route length from $L_{DC,s}$ for scenario evaluation; $V_{dc,nom}$ denotes the rated PV-string DC voltage; and the factor 2 accounts for the positive and negative conductors in the DC loop.

The corresponding AC voltage-drop constraint is expressed by Equation (14):

$$\Delta V_{ac} = \frac{\sqrt{3} \cdot I_{ac} \cdot R_{ac} \cdot L_{ac} \cdot \cos\phi}{V_{ac,nom}} \times 100\% \le 1\% \tag{14}$$

where $I_{ac}$ denotes the rated AC cable current; $R_{ac}$ denotes the AC cable resistance per unit length; $L_{ac}$ is set equal to the applicable scenario-dependent route length from $L_{AC,s}$; $\cos\phi$ denotes the inverter output power factor; $V_{ac,nom}$ denotes the rated AC system voltage; and $\sqrt{3}$ is the three-phase coefficient.

### *3.3. Optimization of Photovoltaic Power Plant Collection Cables Based on NSGA-II*

The physical AC and DC cable losses are converted into a present-value economic cost over the design life. Cable investment and life-cycle power-loss cost are retained as separate objectives so that their trade-off can be represented by a Pareto set. The present-value power-loss cost is calculated using Equation (15):

$$P_{cost} = (P_{1oss,dc} + P_{1oss,ac}) \times T_{op} \times c_{elec} \times \frac{(1+r)^n - 1}{r(1+r)^n} \tag{15}$$

where $c_{elec}$ denotes the electricity price; $T_{op}$ denotes the annual equivalent full-load hours; $r$ denotes the discount rate; and *n* denotes the design service life.

Cable investment and present-value power-loss cost are treated as independent objectives. The multi-objective formulation is given in Equation (16):

$$\min \begin{cases} f_1(x) = C_{ac} + C_{dc} \\ f_2(x) = P_{\text{cost}} \end{cases} \tag{16}$$

(1) Pareto-based multi-objective formulation

In a multi-objective problem, improving one objective may degrade another. In the present application, for example, reducing cable investment can increase the present value of line losses. Equation (16) therefore defines two independent objectives, and the optimization seeks solutions for which neither objective can be improved without worsening the other.

These trade-off solutions constitute the Pareto-optimal set. For the two objectives $f_1(x)$ and $f_2(x)$, Pareto dominance is defined by Equation (17):

$$(vi \in 1,2, f_i(\overline{X}_v) \le f_i(\overline{X}_u)) \Lambda (\exists i \in 1,2, f_i(\overline{X}_v) < f_i(\overline{X}_u)) \tag{17}$$

where $\overline{X}_u$ denotes a Pareto-optimal solution. Candidate solution A dominates solution B if it is no worse in either objective and strictly better in at least one. Nondominated sorting removes dominated layouts and retains the candidate layouts that form the approximate Pareto front.

(2) Optimal design of collector cables based on NSGA-II

Figure 6 summarizes the optimization procedure. The plant capacity, PV-module layout, candidate inverter positions, CAD route polylines, and inter-block boundaries are first defined. Equations (2)–(4) are then used to compute the route-specific serviceable cable lengths for the selected allowance scenario. Cable investment and present-value line-loss cost are evaluated using the objective functions in Equation (16). NSGA-II initializes a population of feasible layouts, generates offspring through crossover and mutation, merges the parent and offspring populations, and ranks the combined population using fast nondominated sorting and crowding distance. Elitist selection produces the next generation, and the procedure continues until the specified iteration limit is reached.

The final nondominated set provides alternative inverter locations with different cable-investment and loss-cost trade-offs. A representative layout is then selected for engineering comparison.

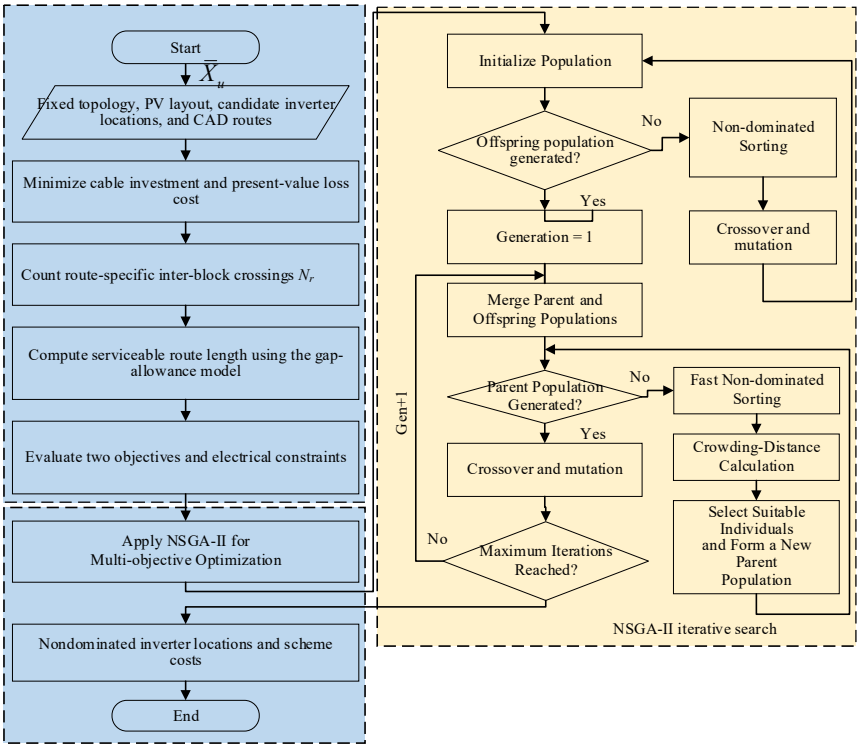


**Figure 6.** NSGA-II procedure for evaluating inverter-location layouts using route-specific serviceable cable lengths, electrical constraints, and two economic objectives.

NSGA-II is employed as a mature multi-objective solver: feasible layouts are ranked by fast nondominated sorting and crowding distance, simulated-binary crossover and polynomial mutation generate offspring, and parent-offspring elitist selection forms the next population. The retained calculation record specifies a population size of 50, a maximum of 600 generations, fast nondominated sorting, crowding-distance selection, simulated-binary crossover, and polynomial mutation.

## 4. Case Study, Results, and Discussion

The overall layout of the offshore floating photovoltaic power station is shown in Figure 7.

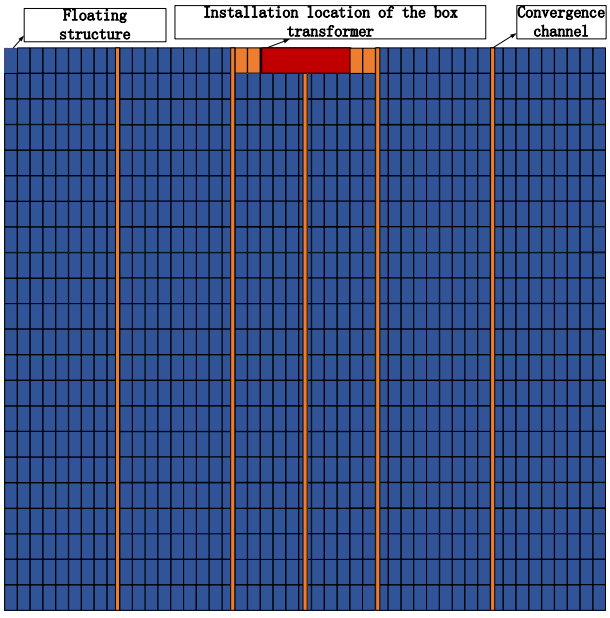


**Figure 7.** Plan layout of the case-study OFPV plant.

The proposed method is applied to a 5.1212 MWp offshore floating photovoltaic plant. As shown in Figure 7: blue regions denote PV-module fields, orange lines denote collection channels and candidate inverter corridors, and red blocks denote the two fixed transformer locations. This representation links the physical plant layout to the routing variables and feasibility constraints used in the optimization.

The installed capacity of the project is 5.1212 MWp. The case comprises 14 generating arrays, two 2500 kVA box-type transformers, and two 35 kV collector feeders. Each feeder connects to a 35 kV branch box. Table 1 lists the string-inverter specifications used in the calculation.

**Table 1.** Main parameters of the string inverter.

| Name | Technical Parameters |
|---|---|
| Rated DC voltage | 1080 V |
| MPPT Voltage Range | 500–1500 V |
| Number of MPPTs | 6 (4/5/5/4/5/5) |
| Maximum Input Current per MPPT | 65 A |
| Rated Output Power | 300 kW |
| Maximum Output Power | 330 kW |
| Degree of Protection | IP66 or higher |

The project contains 1020 floating blocks and 8680 installed PV modules. Figure 8 shows a representative standard block carrying nine modules; it is not a multiplier for the plant-wide module count. Some floating-block positions are used for the two box-type transformers, so nine modules are not installed on every block. The value of 8680 modules in Table 2 is therefore the correct installed quantity. The two transformer outgoing circuits connect through two 35 kV branch boxes to the new 35 kV switch station, as shown in Figure 9.

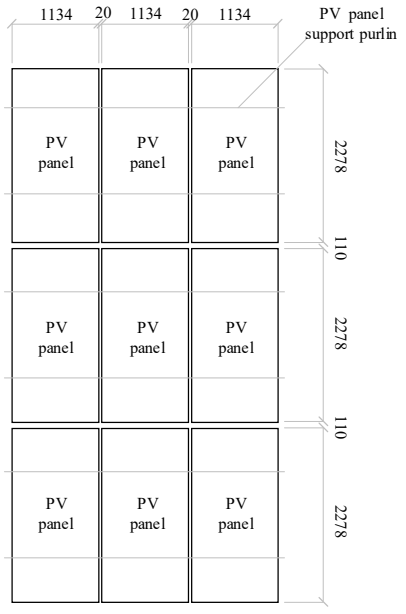


**Figure 8.** PV-module arrangement on a representative floating unit.

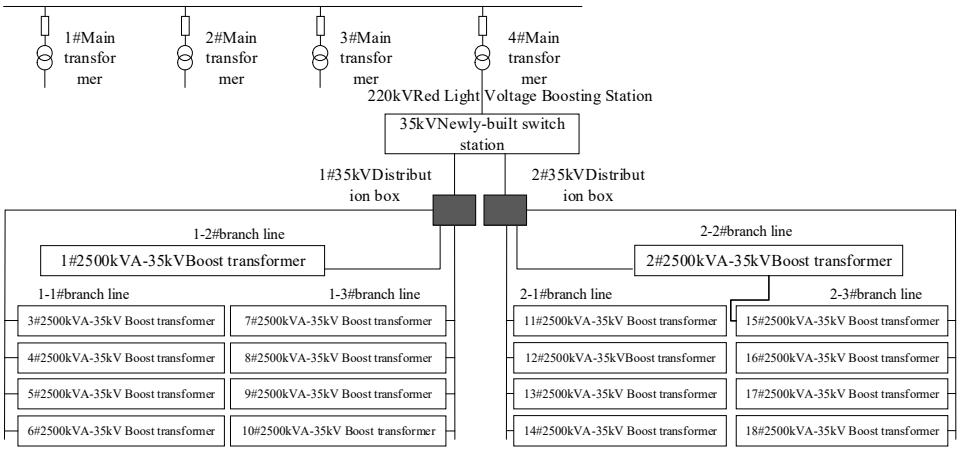


**Figure 9.** Electrical topology of the case-study OFPV plant.

### *4.1. Site Conditions and Generating-Array Data*

The case-study site is in Kenli District, Dongying, China, with a center coordinate of 118.991° E, 37.531° N. The plant center is approximately 4.0 km offshore. The 5 MW implementation area measures about 357.102 m by 317.022 m and occupies 11.3209 ha; the installed capacity evaluated in this study is 5.1212 MWp. The 50-year water-depth range is 1.25–6.64 m, the 50-year daily maximum wind speed is 32.63 m/s, and the maximum current speed is 1.378 m/s.

These data describe the site-selection boundary that precedes the electrical optimization. Candidate OFPV sites should first be screened for available sea area, solar resource, water depth, and seabed conditions, wind-wave-current and sea-ice extremes, navigation and maintenance access, cable landfall and grid connection, environmental effects, and compatibility with other sea uses. The method proposed here is applied only after this screening and optimizes inverter locations and low-voltage cable routes within an approved plant boundary; it does not replace regional offshore site selection.

The generating-array partition is treated as a fixed project input. The 14 arrays are formed to preserve electrical isolation, maintain accessible cable corridors, and match the installed PV capacity to the selected inverter rating. Table 2 reports the actual string count, module count, installed capacity, inverter count, and capacity ratio of each array; these project-specific values, rather than a generic solar-resource-class rule, are used in the optimization.

The plant is divided into 14 generating arrays. Within each array, modules are connected in series to form photovoltaic strings, and the strings are connected in parallel to one string inverter. The 14 inverter outputs are routed through collection channels to the two box-type transformers. The layout within the photovoltaic power station is shown in Figure 10. Table 2 gives the string count, module count, installed capacity, inverter count, and capacity ratio of each array.

**Table 2.** Capacity allocation of the 14 generating arrays.

| Division of Project Areas for This Period | Number of Strings | Number of PV Modules | PV Capacity (Wp) | Number of Inverters | Capacity Ratio |
|---|---|---|---|---|---|
| 1 | 24 | 624 | 368,160 | 1 | 1.227 |
| 2 | 25 | 650 | 383,500 | 1 | 1.278 |
| 3 | 24 | 624 | 368,160 | 1 | 1.227 |
| 4 | 24 | 624 | 368,160 | 1 | 1.227 |
| 5 | 24 | 584 | 344,560 | 1 | 1.149 |
| 6 | 25 | 650 | 383,500 | 1 | 1.278 |
| 7 | 24 | 584 | 344,560 | 1 | 1.149 |
| 8 | 24 | 624 | 368,160 | 1 | 1.227 |

| | | | | | |
|---|---|---|---|---|---|
| 9 | 25 | 650 | 383,500 | 1 | 1.278 |
| 10 | 24 | 624 | 368,160 | 1 | 1.227 |
| 11 | 24 | 624 | 368,160 | 1 | 1.227 |
| 12 | 24 | 584 | 344,560 | 1 | 1.149 |
| 13 | 25 | 650 | 383,500 | 1 | 1.278 |
| 14 | 24 | 584 | 344,560 | 1 | 1.149 |
| Total | 340 | 8680 | 5,121,200 | 14 | —— |

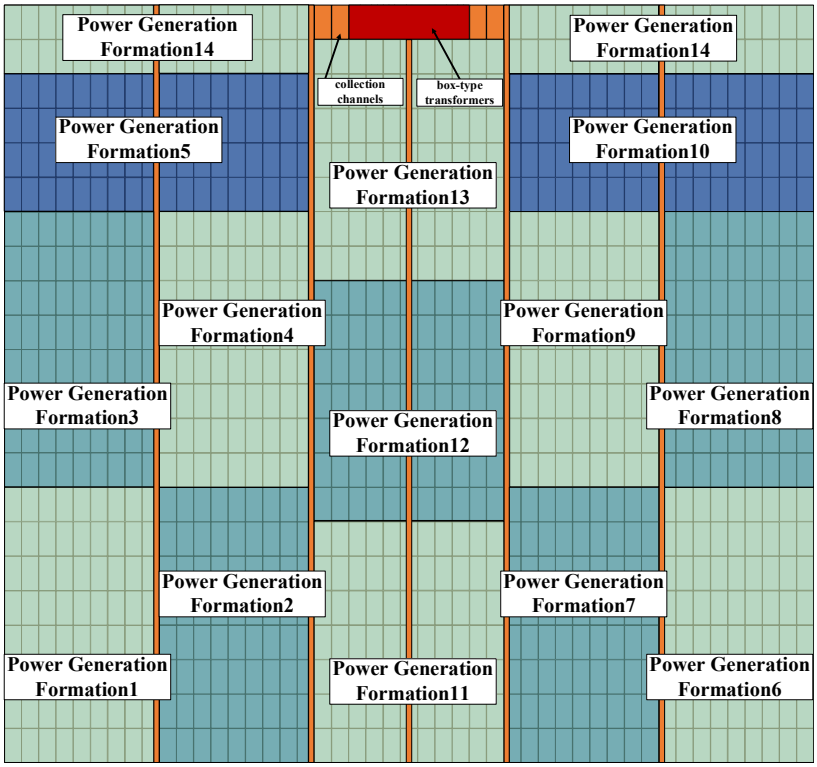


**Figure 10.** Division of the OFPV plant into 14 generating arrays.

Figure 10 confirms the grouping of the 14 arrays around the two fixed transformer locations. With the array partition fixed, the inverter location within each array is the optimization variable. For each candidate position, the model calculates the DC cable length from the PV strings to the inverter and the AC cable length from the inverter to the transformer using the route-specific gap-allowance model. The resulting chromosome is defined by Equation (18):

$$X = I_{1,p}, I_{2,p}, \cdots, I_{14,p}, M_{1,1}, M_{1,2}, \cdots, M_{14,p} \tag{18}$$

where $I$ denotes the DC cable length associated with inverter placement in the mth generating array; $M$ denotes the corresponding AC cable length for the mth generating array; the system contains 14 generating arrays, and $p$ denotes the candidate inverter position.

### *4.2. Optimization Settings and Pareto-Front Results*

Table 3 lists the electrical-economic inputs and the environmental design basis for the case study. Cable prices, economic assumptions, operating hours, nominal route geometry, and $\gamma_s$ enter the electrical-economic formulation. The wave, water-depth, wind, current, and offshore-distance values define the site and mechanical design context; they are not used as direct numerical inputs to the electrical optimization. All reported Pareto fronts and cost comparisons use the nominal inter-block geometry ($\gamma_s = 1$).

**Table 3.** Case-study parameters and environmental design basis.

| Parameter | Value |
|---|---|
| DC cable price, $P_{dc}$ | RMB 6/m |
| AC cable price, $P_{ac}$ | RMB 350/m |
| Discount rate, $r$ | 10% |
| Service life, $n$ | 25 years |
| Electricity price | RMB 0.8/kWh |
| Equivalent full-load hours (h/year) | 1200–1400 |
| Nominal inter-block gap, $d_0$ | 0.05 m |
| Gap-allowance sensitivity scenarios, $\gamma_s$ | 1.00, 1.25, 1.50, 2.00 |
| Environmental reference | $H_s$ = 2.10 m; $T_p$ = 10.19 s; $H_{max}$ = 3.50 m |
| Water-depth range, 50-year conditions | 1.25–6.64 m |
| Daily maximum wind speed, 50-year return period | 32.63 m/s |
| Maximum current speed | 1.378 m/s |
| Distance from shore | Approximately 4.0 km |

Table 3 uses a DC-cable price of RMB 6/m, an AC-cable price of RMB 350/m, a 10% discount rate, a 25-year service life, an electricity price of RMB 0.8/kWh, and 1200–1400 equivalent full-load hours per year. The nominal prototype inter-block gap is 0.05 m. The environmental entries define the mechanical design boundary and do not determine $\gamma_s$ or enter the electrical objectives and constraints directly. The $\gamma_s$ values are prospective design-allowance cases; all reported Pareto and cost results use $\gamma_s = 1$.

For each layout, cable cost and lifetime power-loss cost are calculated from the nominal CAD route lengths and the electrical parameters. The Pareto fronts, Scheme 3 selection, and cost comparison all correspond to $\gamma_s = 1$. The larger $\gamma_s$ values are a defined extension for future route-by-route sensitivity analysis and are not additional numerical results in the present paper.

For a future allowance analysis, the additional length of route $r$ relative to the nominal drawing is $\Delta L_{r,s} = (\gamma_s - 1) N_r d_0$. Candidate rankings can change only when routes have different inter-block crossing counts. Once finalized, crossing counts or synchronized adjacent-block motion data are available, the same formulation can be evaluated for the proposed $\gamma_s$ cases or replaced by crossing-specific time-domain allowances.

NSGA-II is initialized with 50 randomly generated layouts. At each generation, the parent and offspring populations are merged, fast nondominated sorting and crowding-distance evaluation are applied, and an elitist selection step forms the next parent population. The process is repeated for the iteration counts shown in Figure 11, and the resulting Pareto fronts are compared to assess convergence.

Figure 11 compares the Pareto fronts obtained at different iteration counts. The horizontal axis is the cable cost objective, and the vertical axis is the power-loss cost objective.

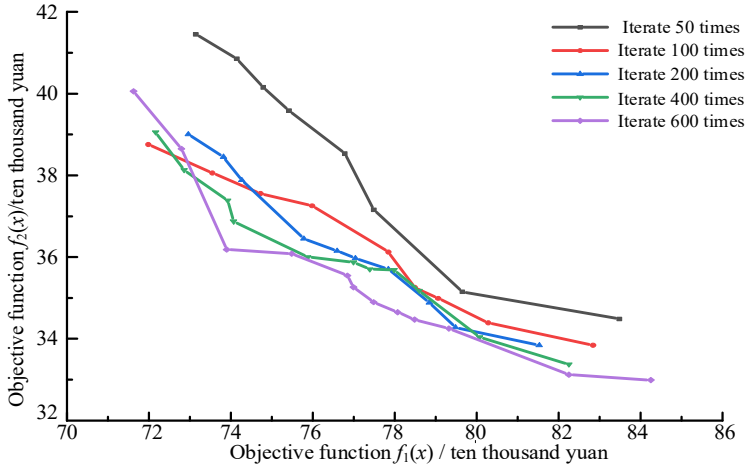


**Figure 11.** Pareto-front convergence at different iteration counts.

Figure 11 shows the expected trade-off between the two objectives: solutions with higher cable expenditure generally have lower power-loss cost. As the iteration count increases, the fronts move toward the lower-loss region and become denser, while the difference between the 400- and 600-iteration fronts becomes small over much of the range. This behavior suggests stabilization of the retained run and supports using the 600-iteration set for the present design comparison; it is not, by itself, proof of a global optimum or run-to-run statistical convergence.

### *4.3. Representative-Scheme Selection and Comparison*

After 600 iterations, the nondominated solution set contains 12 layouts, as summarized in Table 4. Because cable investment and present-value power-loss cost are both expressed in $10^4$ RMB, the representative scheme is selected using the transparent equal-weight total-cost criterion $J = C_{cable} + C_{loss}$, where $C_{cable}$ and $C_{loss}$ are the two cost columns in Table 4. Scheme 3 has $J = 73.89 + 36.18 = 110.07 \times 10^4$ RMB, which is the smallest $J$ among the 12 nondominated layouts. It is therefore selected by a reproducible minimum-total-modeled-cost rule, rather than by visual or subjective preference. Under the same nominal routing convention ($\gamma_s = 1$), Table 5 shows that Scheme 3 reduces cable cost from 79.45 to $73.89 \times 10^4$ RMB (7.0%), power-loss cost from 42.52 to $36.18 \times 10^4$ RMB (14.9%), and total cost from 121.97 to $110.07 \times 10^4$ RMB (9.76%).

**Table 4.** Nondominated solution set after 600 iterations.

| No. | Cable Cost ($10^4$ RMB) | Power-Loss Cost ($10^4$ RMB) |
|---|---|---|
| 1 | 71.62 | 40.05 |
| 2 | 72.79 | 38.64 |
| 3 | 73.89 | 36.18 |
| 4 | 75.48 | 36.08 |
| 5 | 76.84 | 35.54 |
| 6 | 76.99 | 35.26 |
| 7 | 77.48 | 34.89 |
| 8 | 78.07 | 34.64 |
| 9 | 78.48 | 34.46 |
| 10 | 79.32 | 34.25 |
| 11 | 82.25 | 33.12 |
| 12 | 84.25 | 32.99 |

**Table 5.** Comparison of Scheme 3 with the manual design.

| Cost Item | Scheme 3 | Manual Design |
|---|---|---|
| Cable cost ($10^4$ RMB) | 73.89 | 79.45 |
| Power-loss cost ($10^4$ RMB) | 36.18 | 42.52 |
| Total cost ($10^4$ RMB) | 110.07 | 121.97 |

Figure 12 maps the selected chromosome back to the physical layout. The 14 cyan markers identify the selected string-inverter positions, while the orange collection channels and red transformer blocks preserve the fixed electrical topology. The figure provides a direct visual check that the selected solution corresponds to a feasible plant arrangement.

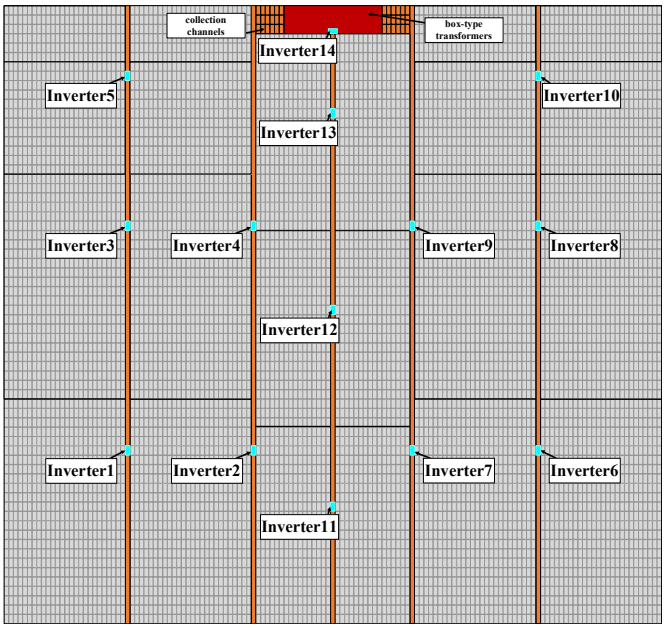


**Figure 12.** Inverter locations in the selected Scheme 3.

### *4.4. Discussion*

The case study confirms that inverter siting affects the two objectives in different ways. The selected Scheme 3 is not claimed to be a universally optimal arrangement: it is the member of the nominal $\gamma_s = 1$ nondominated set that minimizes the explicitly defined equal-weight total modeled cost $J = C_{cable} + C_{loss}$. A different decision-maker weighting of capital expenditure and operating loss could justify another member of the same Pareto set. The larger $\gamma_s$ values remain prospective sensitivity cases and were not used to select or rank Scheme 3 in the present calculation.

Relative to conventional static-distance planning, the proposed formulation makes the location of floating-block interfaces explicit at route level. Its present numerical benefit, however, arises from coordinated inverter siting and nominal CAD-route evaluation because the calculations use $\gamma_s = 1$.

The numerical values are project-specific because the array partition, transformer locations, feeder topology, equipment ratings, cable prices, and operating assumptions are fixed. Transfer to another OFPV plant requires its own CAD routes, floating-block boundaries, conductor data, economic parameters, and electrical constraints. Mechanical design also requires minimum-bending-radius, tension, curvature, and fatigue checks that are outside the present planning-level optimization.

Wind and current can indirectly affect cable routing by changing platform offset, rotation, and relative motion at floating-block interfaces. These effects may alter the required free cable length and the tension, bending, and fatigue demand. The present electrical-economic model does not calculate those mechanical responses; the wind and current values in Table 3 therefore define only the design environment. A quantitative mapping from environmental loads to cable allowance requires coupled hydrodynamic, mooring, and cable analysis.

## 5. Conclusions and Future Work

This study develops a multi-objective design method for inverter placement and low-voltage collector-cable routing in a fixed-topology offshore floating photovoltaic plant. The generating-array boundaries, transformer locations, feeder topology, inverter type, and cable specifications are treated as prescribed inputs, while one feasible inverter location in each array, along with its associated DC and AC routes, is selected. A CAD-informed inter-block gap-allowance model is coupled with cable-investment and present-

value loss-cost objectives, and NSGA-II is used to construct the corresponding nondominated solution set. The principal conclusions are as follows.

(1) The route-specific gap-allowance model distinguishes the cable length fixed to modules, beams, or other supports from the portions that cross floating-block interfaces. Consequently, the additional service allowance depends on the crossing count of each route instead of being imposed through one global wave multiplier. The model recovers the nominal CAD length when $\gamma_s = 1$, leaves routes with no inter-block crossing unchanged, and increases the serviceable length monotonically with $\gamma_s$ for routes that do cross block boundaries. The 0.05 m nominal prototype gap obtained from the 1:25 physical-model geometry provides the dimensional reference, whereas $\gamma_s$ remains a bounded design-allowance parameter rather than a calibrated hydrodynamic coefficient.

(2) Coupling the route model with DC and AC cable investment, resistive losses, and electrical constraints reveals the trade-off between initial expenditure and lifetime operating losses. For the 5.1212 MWp plant, the 600-generation run produces 12 nondominated layouts. Lower loss cost generally requires higher cable investment, so the method provides several feasible alternatives rather than one preference-dependent optimum.

(3) Scheme 3 is selected from the nominal $\gamma_s = 1$ nondominated set by minimizing $J = C_{cable} + C_{loss}$. Relative to the manual design, its modeled cable cost decreases from $79.45 \times 10^4$ to $73.89 \times 10^4$ RMB (7.0%), and its present-value power-loss cost decreases from $42.52 \times 10^4$ to $36.18 \times 10^4$ RMB (14.9%). The total modeled cost decreases from $121.97 \times 10^4$ to $110.07 \times 10^4$ RMB, a reduction of 9.76%. All quantitative results use $\gamma_s = 1$. Future work will use measured or simulated relative motions to evaluate route-specific dynamic allowances.

(4) The 5.1212 MWp case is derived from an actual offshore floating photovoltaic engineering project, and the proposed method was applied during its electrical-layout design. The 9.76% reduction relative to the manual scheme provides engineering evidence of the method's effectiveness for the present project. The formulation is not tied to this capacity: a larger fixed-topology plant can be represented by extending the sets of generating arrays, candidate inverter positions, transformer nodes, and feasible cable routes without changing the basic model. However, complete layout and electrical-routing data for larger offshore floating photovoltaic projects are currently difficult to obtain because the technology remains at an early stage of engineering development, and detailed project data are rarely publicly available. The present result should therefore not be extrapolated directly to larger plants. Future work will test the method on a larger engineering project once a sufficiently complete dataset becomes available, with particular attention to computational efficiency, convergence performance, and economic benefits.

## Author Contributions

Conceptualization, Y.Z., P.L. and X.K.; Methodology, Y.Z., P.L. and Z.Y. (Zilong Yu); Software, Z.Y. (Zilong Yu), P.L. and X.K.; Validation, Y.Z. and P.L.; Formal Analysis, Y.Z., P.L. and X.K.; Investigation, Y.Z. and Z.Y. (Zilong Yu); Resources, X.K., P.L. and Y.Z.; Data Curation, Y.Z. and Z.Y. (Zilong Yu); Writing—Original Draft Preparation, Y.Z., P.L. and Z.Y. (Zilong Yu); Writing—Review & Editing, X.K., P.L. and Z.Y. (Zilong Yu).; Visualization, Y.Z. and Z.Y. (Zhenglong Yang); Supervision, X.K., P.L. and Z.Y. (Zhenglong Yang); Project Administration, P.L., X.K. and Z.Y. (Zhenglong Yang); Funding Acquisition, P.L. All authors have read and agreed to the published version of the manuscript.

## Ethics Statement

Not applicable.

## Informed Consent Statement

Not applicable.

## Data Availability Statement

Data will be made available on request.

## Funding

This research was funded by the National Natural Science Foundation of China, grant number 52507138.

## Declaration of Competing Interest

The authors declare that they have no known competing financial interests or personal relationships that could have appeared to influence the work reported in this paper.

## References

1. Sahu A, Yadav N, Sudhakar K. Floating photovoltaic power plant: A review. *Renew. Sustain. Energy Rev.* **2016**, *66*, 815–824. DOI:10.1016/j.rser.2016.08.051
2. Ranjbaran P, Yousefi H, Gharehpetian GB, Astaraei FR. A review on floating photovoltaic (FPV) power generation units. *Renew. Sustain. Energy Rev.* **2019**, *110*, 332–347. DOI:10.1016/j.rser.2019.05.015
3. Claus R, López M. Key issues in the design of floating photovoltaic structures for the marine environment. *Renew. Sustain. Energy Rev.* **2022**, *164*, 112502. DOI:10.1016/j.rser.2022.112502
4. Tang Y, Chen X, Huang G, Chen M, Zhang K, Jiang Y, et al. Dynamic analysis of multi-module floating photovoltaic platforms with composite mooring system considering tidal variation and platform configuration. *Ocean Eng.* **2024**, *312*, 119243. DOI:10.1016/j.oceaneng.2024.119243
5. Shi Y, Wei Y, Chen Z. Analysis of hydroelastic response and failure mechanisms of floating offshore photovoltaic under wind and wave. *Ocean Eng.* **2025**, *328*, 121028. DOI:10.1016/j.oceaneng.2025.121028
6. Du J, Zhang D, Zhang Y, Xu K, Chang A, Zhao S. Design and comparative analysis of alternative mooring systems for offshore floating photovoltaics arrays in ultra-shallow water with significant tidal range. *Ocean Eng.* **2024**, *302*, 117649. DOI:10.1016/j.oceaneng.2024.117649
7. Luo W, Zhang X, Tian X, Cheng Z, Wen B, Li X, et al. Conceptual design and model test of a pontoon-truss type offshore floating photovoltaic system with soft connection. *Ocean Eng.* **2024**, *309*, 118518. DOI:10.1016/j.oceaneng.2024.118518
8. Ahmad IB, Schnepf A, Ong MC. An optimisation methodology for suspended inter-array power cable configurations between floating offshore wind turbines. *Ocean Eng.* **2023**, *278*, 114406. DOI:10.1016/j.oceaneng.2023.114406
9. Tabi Fouda BM, Han D, Zhang W, An B. Research on key technology to determine the exact maximum allowable current-carrying ampacity for submarine cables. *Opt. Laser Technol.* **2024**, *175*, 110705. DOI:10.1016/j.optlastec.2024.110705
10. Cazzaniga R, Cicu M, Rosa-Clot M, Rosa-Clot P, Tina G, Ventura C. Floating photovoltaic plants: Performance analysis and design solutions. *Renew. Sustain. Energy Rev.* **2018**, *81*, 1730–1741. DOI:10.1016/j.rser.2017.05.269
11. Ferrer-Gisbert C, Ferrán-Gozálvez JJ, Redón-Santafé M, Ferrer-Gisbert P, Sánchez-Romero FJ, Torregrosa-Soler JB. A new photovoltaic floating cover system for water reservoirs. *Renew. Energy* **2013**, *60*, 63–70. DOI:10.1016/j.renene.2013.04.007
12. Wędzik A, Szypowski M, Siewierski T. An integrated method to simultaneously optimise a wind farm internal network layout, cable cross-sections and substation location. *Appl. Energy* **2025**, *377*, 124361. DOI:10.1016/j.apenergy.2024.124361
13. Zhang L, Wang J, Jiao H, Du J, Li M. Economical sizing and configuration optimization of floating offshore photovoltaic systems using NSGA-II. *Ocean Eng.* **2025**, *328*, 120836. DOI:10.1016/j.oceaneng.2025.120836
14. Pillai A, Chick J, Johanning L, Khorasanchi M, de Laleu V. Offshore wind farm electrical cable layout optimization. *Eng. Optim.* **2015**, *47*, 1689–1708. DOI:10.1080/0305215X.2014.992892
15. Pereira JLJ, Oliver GA, Francisco MB, Cunha SS, Gomes GF. A review of multi-objective optimization methods and algorithms. *Arch. Comput. Methods Eng.* **2022**, *29*, 2285–2308. DOI:10.1007/s11831-021-09663-x
16. Verma S, Pant M, Snasel V. A comprehensive review on NSGA-II for multi-objective combinatorial optimization problems. *IEEE Access* **2021**, *9*, 57757–57791. DOI:10.1109/ACCESS.2021.3070634

17. Deb K, Pratap A, Agarwal S, Meyarivan T. A fast and elitist multiobjective genetic algorithm: NSGA-II. *IEEE Trans. Evol. Comput.* **2002**, *6*, 182–197. DOI:10.1109/4235.996017
18. Peng Y, Zeng T, Fan L, Han Y, Xia B. An improved genetic algorithm-based robust approach for stochastic dynamic facility layout problems. *Discrete Dyn. Nat. Soc.* **2018**, *2018*, 1–8. DOI:10.1155/2018/1529058
19. Hao J, Yang X, Wang C, Tu R, Zhang T. An improved NSGA-II algorithm based on adaptive weighting and searching strategy. *Appl. Sci.* **2022**, *12*, 11573. DOI:10.3390/app122211573
20. Liu H, Li Y, Duan Z, Chen C. A review on multi-objective optimization framework in wind energy forecasting techniques and applications. *Energy Convers. Manag.* **2020**, *224*, 113324. DOI:10.1016/j.enconman.2020.113324
21. Gurfude SS, Bhavitha C, Tanusha D, Mounika D, Gouda Kake SP, SaiSudha M, et al. Techno-economic analysis of a 1 MWp floating solar PV plant. In Proceedings of the 2020 IEEE First International Conference on Smart Technologies for Power, Energy and Control (STPEC), Nagpur, India, 25–26 September 2020; pp. 1–6. DOI:10.1109/STPEC49749.2020.9297740
22. Dzamesi SKA, Ahiataku-Togobo W, Yakubu S, Acheampong P, Kwarteng M, Samikannu R, et al. Comparative performance evaluation of ground-mounted and floating solar PV systems. *Energy Sustain. Dev.* **2024**, *80*, 101421. DOI:10.1016/j.esd.2024.101421
23. Schnepf A, Lopez-Pavon C, Ong MC, Yin G, Johnsen Ø. Feasibility study on suspended inter-array power cables between two spar-type offshore wind turbines. *Ocean Eng.* **2023**, *277*, 114215. DOI:10.1016/j.oceaneng.2023.114215
24. Beier D, Ong MC, Janocha MJ, Ye N. Application of suspended inter-array power cables in floating offshore wind farms. *Appl. Ocean Res.* **2024**, *147*, 103991. DOI:10.1016/j.apor.2024.103991
25. Ménard F, Cartraud P. A computationally efficient finite element model for the analysis of the non-linear bending behaviour of a dynamic submarine power cable. *Mar. Struct.* **2023**, *91*, 103465. DOI:10.1016/j.marstruc.2023.103465
26. Okoro A, Khan F, Ahmed S. Dependency effect on the reliability-based design optimization of complex offshore structure. *Reliab. Eng. Syst. Saf.* **2023**, *231*, 109026. DOI:10.1016/j.ress.2022.109026
27. Rentschler MU, Adam F, Chainho P. Design optimization of dynamic inter-array cable systems for floating offshore wind turbines. *Renew. Sustain. Energy Rev.* **2019**, *111*, 622–635. DOI:10.1016/j.rser.2019.05.024